Journal Pre-proof

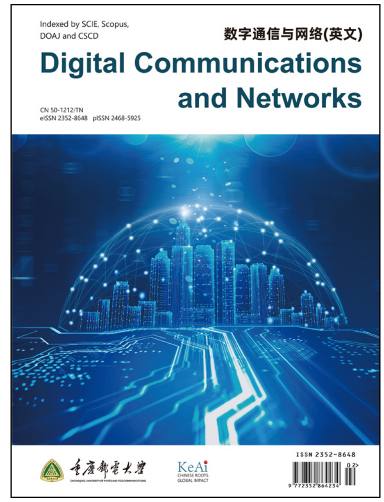

Performance analysis of RIS-assisted dual-hop mixed FSO-RF UAV communication systems

Donghyun Kim, Hwi Sung Park and Bang Chul Jung

PII: S2352-8648(25)00006-9
DOI: https://doi.org/10.1016/j.dcan.2025.02.001
Reference: DCAN 845

To appear in: *Digital Communications and Networks*

Received date: 10 July 2024
Revised date: 27 January 2025
Accepted date: 20 February 2025

Please cite this article as: D. Kim, H.S. Park and B.C. Jung, Performance analysis of RIS-assisted dual-hop mixed FSO-RF UAV communication systems, *Digital Communications and Networks*, doi: https://doi.org/10.1016/j.dcan.2025.02.001.

Digital Communications and Networks(DCN)

HOSTED BY

ELSEVIER

Available online at www.sciencedirect.com

ScienceDirect

journal homepage: www.elsevier.com/locate/dcan

DCN Digital Communications and Networks

Performance analysis of RIS-assisted dual-hop mixed FSO-RF UAV communication systems

Donghyun Kim[a], Hwi Sung Park[a], Bang Chul Jung[b,*]

[a] **Agency for Defense Development, Daejeon 34186, South Korea**
[b] **Department of Electrical and Computer Engineering, Ajou University, Suwon 16499, South Korea**

Abstract

In this paper, we investigate a Reconfigurable Intelligent Surface (RIS)-assisted Free-Space Optics–Radio Frequency (FSO–RF) mixed dual-hop communication system for Unmanned Aerial Vehicles (UAVs). In the first hop, a source UAV transmits data to a relay UAV using the FSO technique. In the second hop, the relay UAV forwards data to a destination Mobile Station (MS) via an RF channel, with the RIS enhancing coverage and performance. The relay UAV operates in a Decode-and-Forward (DF) mode. As the main contribution, we provide a mathematical performance analysis of the RIS-assisted FSO–RF mixed dual-hop UAV system, evaluating outage probability, Bit-Error Rate (BER), and average capacity. The analysis accounts for factors such as atmospheric attenuation, turbulence, geometric losses, and link interruptions caused by UAV hovering behaviors. To the best of our knowledge, this is the first theoretical investigation of RIS-assisted FSO–RF mixed dual-hop UAV communication systems. Our analytical results show strong agreement with Monte Carlo simulation outcomes. Furthermore, simulation results demonstrate that RIS significantly enhances the performance of UAV-aided mixed RF/FSO systems, although performance saturation is observed due to uncertainties stemming from UAV hovering behavior.

KEYWORDS: Unmanned aerial vehicle, Free-space optics, Reconfigurable intelligent surface, Mixed RF/FSO channel, Outage probability, Bit-error rate.

1. Introduction

1.1. Literature Review

Reconfigurable Intelligent Surface (RIS) has garnered significant attention as a promising technology for next-generation wireless systems, including beyond fifth-generation (B5G) and sixth-generation (6G) networks [1, 2, 3, 4, 5, 6, 7]. The RIS dynamically adjusts the amplitude and phase of incident signals through software-controlled reflections on passive elements, enabling reflective beamforming [1]. In [2], various RIS-based communication scenarios have been explored, including applications for users in dead zones or at cell edges, physical-layer security, and massive Device-to-Device (D2D) communications. For these scenarios, Wu and Zhang [2] presented the fundamental hardware architecture, beamforming challenges, and various numerical results demonstrating signal power enhancement and interference suppression facilitated by the RIS. Additionally, in [6], RIS was applied to mmWave integrated sensing and communication systems. In [7], RIS-enabled satellite-aerial-terrestrial networks utilizing Power-Domain Non-Orthogonal Multiple Access (PD-NOMA) were introduced, showcasing various practical application scenarios. Moreover, RIS has been applied to homogeneous cooperative communication systems [4] as well as Free-Space Optics (FSO)/Radio Frequency (RF) mixed cooperative communication systems [3, 5].

On the other hand, FSO communication is regarded as a promising technology for future wireless backhaul and fronthaul networks, owing to its license-free operation and low-interference characteristics [8]. The mixed dual-hop FSO/RF Amplify-Forward (AF) re-

*Corresponding author
[1]Email addresses: dh-kim@add.re.kr (D. Kim), winzip90@kaist.ac.kr (H. S. Park), bcjung@ajou.ac.kr (B. C. Jung)

laying communication system has been proposed as an adaptive and efficient technique for practical wireless communication systems, with its performance analyzed mathematically [9]. Recently, the mixed FSO/RF scheme has been incorporated into Space-Air-Ground Integrated Networks (SAGINs), taking into account a practical FSO channel model that includes Angle-of-Arrival (AoA) fluctuations [10].

Unmanned Aerial Vehicles (UAVs) are considered a key component of future mobile communication systems due to their ease of deployment and virtually limitless flexibility [13]. If UAVs rely solely on RF links, they are likely to encounter interference between backhaul and access links. To address this, the mixed FSO-RF approach is considered a promising solution for UAV-assisted systems. However, the inherent instability of UAVs can significantly degrade end-to-end communication performance. An accurate UAV-based FSO channel model has been studied, accounting for UAV hovering and incorporating the combined effects of atmospheric turbulence, as well as the position and AoA of UAVs [11, 14, 15]. The channel model was further refined in [16] by incorporating a generalized Málaga channel to represent the FSO atmospheric turbulence. Additionally, a decode-and-forward (DF) protocol-based mixed FSO-RF relaying technique was proposed, where the end-to-end performance was analyzed; however, the analysis relied on a simplified channel model for UAVs [16]. On the other hand, various RIS-assisted UAV systems have been proposed, such as RIS-carrying UAVs and RIS-assisted UAVs, along with joint trajectory and beamforming optimization [17]. In [18], a RIS-aided symbiotic transmission approach was introduced, incorporating trajectory and phase-shift optimization.

1.2. Motivations and Contributions

- We consider a RIS-assisted dual-hop mixed FSO-RF system, where a single hovering UAV operates as a relay using the DF protocol. However, prior works such as [14, 19, 20] focused solely on pure FSO or RF links. While [21] explores a mixed FSO-RF channel model, it does not account for interruptions caused by UAV behavior or the performance enhancements enabled by RISs.

- As the main contribution of this paper, we mathematically analyze the end-to-end outage probability, Bit-Error Rate (BER), and achievable rate performance under a practical channel model that accounts for atmospheric loss, turbulence loss, geometrical loss, and AoA-induced loss. Although [19] introduced a more sophisticated UAV FSO channel model [11, 14], we adopted the model from [11] due to its balance of simplicity and sufficient accuracy.

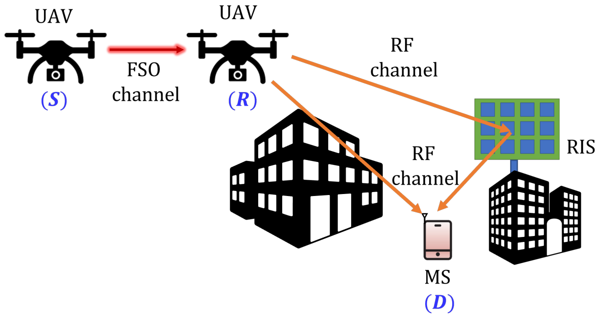

Fig. 1. System model of the RIS-assisted Dual-Hop mixed FSO-RF UAV Communication System.

- To the best of our knowledge, the performance analysis of mixed RF/FSO systems that considers both UAV-induced instability in the FSO channel and RIS-assisted RF channels, with or without a direct path component, has not yet been reported in the literature. Building on previous works on FSO channels [11] and RIS-assisted RF channels [12], as well as further investigations into RIS-assisted channel performance with and without a direct path, we evaluated the end-to-end performance of the proposed system model. Furthermore, prior studies have not provided BER analysis for general M-ary Quadrature Amplitude Modulation (M-QAM) systems or examined the average capacity of RIS links. A detailed comparison with related literature is summarized in Table 1.

- Through extensive computer simulations, we demonstrate that the results hold across all SNR regimes.

The remainder of this paper is organized as follows: Section 2 introduces the RIS-assisted mixed FSO/RF DF relaying system. In Section 3, we mathematically analyze the outage probability, BER, and average capacity of the UAV-aided DF relaying system. Section 4 presents simulation results for scenarios with and without a direct RF path, and conclusions are provided in Section 5.

2. System and Channel Models

Figure 1 illustrates the RIS-assisted dual-hop mixed FSO-RF UAV communication system considered in this paper. The system comprises a single source node (S), a single DF relay (R), and a single destination node (D). The source and relay nodes are assumed to be UAVs, while the destination node represents a Mobile Station (MS). It is further assumed that there is no direct communication link between the source and destination nodes. To provide a practical perspective on the proposed model, consider the following usage scenario: one UAV acts as a traffic-generating source

Ref.	Hops	Optical Link	RIS Link	Direct RF-Path	RF Analysis Approach
[3]	Dual Hop	Fixed FSO	Rayleigh, Rayleigh	NO	CLT based
[4]	Single Hop	NO	$k-\mu$	NO	Exact PDF calculation
[6]	Single Hop	NO	mmWave	YES	Exact PDF calculation
[7]	Single Hop	NO	various	NO	NO (Survey Paper)
[10]	Dual Hop	UAV FSO	NO	Shadowed Rician	Exact PDF calculation
[11]	Single Hop	UAV FSO	NO	N/A	N/A
[12]	Single Hop	NO	Rayleigh, Rayleigh	NO	PDF approximation
This Work	Dual Hop	UAV FSO	Nakagami-*m*, Rayleigh	generalized-K	PDF approximation

Table 1
Comparison our manuscript with the existing studies

(e.g., video streaming), while the other UAV functions as a relay unit for serving multiple mobile users.

It is assumed that the link between the source and relay nodes operates over an FSO channel, while the link between the relay and destination nodes utilizes an RF channel. A single RIS is positioned between the relay and destination nodes to enhance the RF link. In this paper, we adopt a practical FSO channel model that accounts for atmospheric loss, turbulence, Angle-of-Arrival (AoA) fluctuations, and geometrical loss caused by misalignment between the lens center and beam center, as described in [11, 15]. We assume *full* channel state information (CSI) at the RIS, following the approach in [4]. The RF channel between the relay node and the RIS (R-RIS) is modeled using a Nakagami-*m*[2] distribution, while the channel between the RIS and the destination node (RIS-D) follows a Rayleigh distribution. For the R-RIS channel, we utilize the Nakagami-*m* distribution, as it effectively captures the Line-of-Sight (LoS) contribution, reflecting the UAV's ability to fly above buildings. In contrast, for the RIS-D channel, we employ the Rayleigh distribution, which assumes a non-LoS channel, aligning with the typical deployment of MSs on the ground. Moreover, we assume the existence of an RF direct link between the relay UAV and the MS, modeled using a generalized-K (K_G) distribution, as it effectively captures both fading and shadowing effects. While Malaga and $\kappa-\mu$ distributions can model various fading scenarios in FSO and RF channels, they are relatively complex for analytical purposes. As a more practical alternative, we adopt Gamma-Gamma, Nakagami-*m*, Rayleigh, and generalized-K (K_G) channel models, which are simpler yet sufficiently accurate for gaining insights into the UAV-aided mixed RF-FSO channel model.

2.1. First time-slot: FSO link

In the first time slot, the source node sends signal x_{FSO} with the energy of $E_{\text{FSO}} \triangleq \mathbb{E}[|x_{\text{FSO}}|^2]$ to the relay node via UAV-UAV FSO link. After filtering the Direct Current (DC) component at the relay node, the received signal is given by [3]

$$y_{\text{FSO}} = \eta h_{\text{FSO}} x_{\text{FSO}} + n_{\text{FSO}}, \tag{1}$$

where h_{FSO}, n_{FSO}, η represent the FSO channel gain, complex Gaussian FSO receiver noise following $\mathcal{CN}(0, N_{\text{FSO}})$, and effective photoelectric conversion ratio, respectively. The FSO channel gain is typically modeled as [15]

$$h_{\text{FSO}} = h_p^{\text{FSO}} h_a^{\text{FSO}} h_{pg}^{\text{FSO}} h_{pa}^{\text{FSO}}, \tag{2}$$

where $h_p^{\text{FSO}} = \exp(-D_{\text{FSO}}\xi)$ represents atmospheric loss, with ξ as scattering coefficient and D_{FSO} as the distance between source and relay nodes. h_a^{FSO} accounts for atmospheric turbulence, modeled using Gamma-Gamma fading. h_{pg}^{FSO} represents geometrical loss caused by the misalignment between the receiver lens center and the beam center, and h_{pa}^{FSO} captures link interruptions due to AoA fluctuations. Based on this channel model, the average SNR is given by [15]

$$\begin{aligned} \bar{\gamma}_{FSO} &= \frac{\eta^2(\mathbb{E}[h_{FSO}])^2 E_{\text{FSO}}}{N_{FSO}} \\ &= \frac{\eta^2 A_0^2 \tau^2 (h_p^{FSO})^2 E_{\text{FSO}}}{(1+\tau)^2 N_{FSO}}, \end{aligned} \tag{3}$$

where $A_0 = (\text{erf}(v))^2$ represents the received optical power, and τ is defined as

$$\tau = \frac{w_{zeq}^2}{4\left(D_{\text{FSO}}^2 \sigma_{to}^2 + \sigma_{tp}^2 + \sigma_{rp}^2\right)}. \tag{4}$$

In (4), w_{zeq}^2 denotes the equivalent beam waist with the beam waist at the receiver w_z, which is formally defined as

$$w_{zeq}^2 = w_z^2 \frac{\sqrt{\pi}\,\text{erf}(v)}{2v\exp(-v^2)}, \tag{5}$$

where $v = \frac{\sqrt{\pi}}{\sqrt{2}w_z} r_a$. The term r_a denotes the receiver lens radius, and $\text{erf}(\cdot)$ denotes the error function. The terms σ_{tp}^2, σ_{rp}^2, and σ_{to}^2 indicate position variation of the transmitter, receiver, and orientation variation of the transmitter, respectively. Then, the instantaneous

[2] It is well known that the Nakagami-*m* distribution closely approximates the Rician-K distribution, with the relationship $m = \frac{(K+1)^2}{(2K+1)}$, effectively capturing the line-of-sight (LoS) effect [22].

SNR is given by

$$\gamma_{\text{FSO}} = \frac{\eta^2 h_{\text{FSO}}^2 E_{\text{FSO}}}{N_{\text{FSO}}} = \left(\frac{(1+\tau)h_a^{\text{FSO}} h_{pg}^{\text{FSO}} h_{pa}^{\text{FSO}}}{A_0 \tau}\right)^2 \bar{\gamma}_{\text{FSO}} \quad (6)$$

and its probability density function (PDF) is given by [15]

$$f_{\gamma_{\text{FSO}}}(\gamma_{\text{FSO}}) \simeq a_1 \delta(\gamma_{\text{FSO}}) + C_1 \gamma_{\text{FSO}}^{-1/2} \times G_{1,3}^{3,0}\left(C_2 \sqrt{\gamma_{\text{FSO}}} \left| \begin{matrix} \tau \\ \tau-1, \alpha-1, \beta-1 \end{matrix} \right.\right)\Bigg], \quad (7)$$

where

$$C_1 = \frac{(1-a_1)\alpha\beta\tau^2}{2(1+\tau)\Gamma(\alpha)\Gamma(\beta)\sqrt{\bar{\gamma}_{FSO}}}, \quad C_2 = \frac{\alpha\beta\tau}{(1+\tau)\sqrt{\bar{\gamma}_{FSO}}}, \quad (8)$$

and $\Gamma(\cdot)$ denotes a gamma random variable, $\delta(.)$ represents dirac-delta function,

$$a_1 = \exp\left(-\frac{\theta_{\text{FOV}}^2}{2\left(\sigma_{to}^2 + \sigma_{ro}^2\right)}\right) \quad (9)$$

with the field-of-view θ_{FOV} and the orientation variation of receiver σ_{ro}^2. With the Rytov variance σ_R^2, α and β denotes small-scale and large-scale fluctuations, which is defined as

$$\alpha = \left[\exp\left(\frac{0.49\sigma_R^2}{(1+1.11\sigma_R^{12/5})^{7/6}}\right) - 1\right]^{-1} \quad (10)$$

and

$$\beta = \left[\exp\left(\frac{0.51\sigma_R^2}{(1+0.69\sigma_R^{12/5})^{5/6}}\right) - 1\right]^{-1}, \quad (11)$$

respectively.

2.2. Second time-slot: RIS-assisted RF link

In the second time slot, the decoded signal $x_{\text{RIS}} = \hat{x}_{\text{FSO}}$ with energy $E_{\text{RIS}} \triangleq \mathbb{E}\{|x_{\text{RIS}}|^2\}$ is transmitted via RF channel and then the received signal at the destination node is given by

$$y_{\text{RIS}} = \left(\sum_{k=1}^{N} h_k v_k g_k + h_d\right) x_{\text{RIS}} + n_{\text{RIS}}, \quad k = 1, 2, ..., N, \quad (12)$$

where the terms $h_k = \alpha_k e^{-j\varphi_k}$, $g_k = \beta_k e^{-j\psi_k}$, and $v_k = e^{j\phi_k}$ denote the channel gains from the relay node to the RIS and the RIS to destination node, and the phase steering contribution of the k-th RIS element with each phase value of φ_k, ψ_k, and ϕ_k, respectively. Moreover, $h_d = \mathcal{H}_d e^{-j\kappa_d}$ denotes channel gain from relay to destination with its phase κ_d. In this paper, we assume that the RIS has N elements. The term α_k is assumed to be Nakagami-m Random Variable (RV) with m_I and β_k is assumed to be Rayleigh RVs with mean 0 and variance 1. The term n_{RIS} denotes the additive white Gaussian noise (AWGN) at the destination node, which follows $\mathcal{CN}(0, N_{\text{RIS}})$.

To maximize the received SNR at the destination node, we set $\phi_k = \varphi_k + \psi_k + \kappa_d$ to align all the phase of channel elements, and then the received signal can be rewritten as

$$y_{\text{RIS}} = \mathcal{H} e^{-j\kappa_d} x_{\text{RIS}} + n_{\text{RIS}}, \quad (13)$$

where $\mathcal{H} = \mathcal{H}_{RIS} + \mathcal{H}_d$, and

$$\mathcal{H}_{RIS} = \sum_{k=1}^{N} \alpha_k \beta_k = \sum_{k=1}^{N} \delta_k \quad (14)$$

denotes the effective channel gain of the RIS link, which can be modeled as a sum of N Independent and Identically Distributed (i.i.d.) RVs, and this can be a sum of K_G random variable δ_k with its Probability Density Function (PDF)

$$f_{\delta_k}(r) = \frac{4 m_I^{\frac{m_I+1}{2}} r^{m_I}}{\Gamma(m_I)} K_{m_I-1}(2\sqrt{m_I} r), \quad (15)$$

where $K_v(\cdot)$ indicates the modified v-order Bessel function of the second kind. Then, the instantaneous SNR at the destination node can be calculated as

$$\gamma_{RIS} = \mathcal{H}^2 \bar{\gamma}_{\text{RIS}}. \quad (16)$$

where $\bar{\gamma}_{\text{RIS}} = \frac{E_{\text{RIS}}}{N_{\text{RIS}}}$ indicates the average SNR in the second hop. According to [12, 23], the sum of i.i.d. multiple K_G random variables is well approximated by the PDF of $\sqrt{W}$ with $W = \sum_{k=1}^{N} \delta_k^2$. Therefore, the PDF of $\mathcal{H}_{RIS}$ can be approximated by

$$f_{\mathcal{H}_{RIS}}(r|k_w, m_w, \Omega_w) \approx \frac{4\Xi^{\zeta_w^+} r^{\zeta_w^+ - 1}}{\Gamma(k_w)\Gamma(m_w)} K_{\zeta_w^-}(2\Xi_w r), \quad (17)$$

where $\zeta_w^- = k_w - m_w$ and $\zeta_w^+ = k_w + m_w$, with $k_w = \frac{-b+\sqrt{b^2-4ac}}{2a}$ and $m_w = \frac{-b-\sqrt{b^2-4ac}}{2a}$ are shaping parameters, $\Xi_w = \sqrt{k_w m_w / \Omega_w}$ and $\Omega_w = \mu_{\mathcal{H}}(2)$ is mean power of $\mathcal{H}_{RIS}$. Moreover, a, b and c are defined as follows:

$$a = \mu_{\mathcal{H}}(6)\mu_{\mathcal{H}}(2) + \mu_{\mathcal{H}}^2(2)\mu_{\mathcal{H}}(4) - 2\mu_{\mathcal{H}}^2(4)$$
$$b = \mu_{\mathcal{H}}(6)\mu_{\mathcal{H}}(2) - 4\mu_{\mathcal{H}}^2(4) + 3\mu_{\mathcal{H}}^2(2)\mu_{\mathcal{H}}(4)$$
$$c = 2\mu_{\mathcal{H}}^2(2)\mu_{\mathcal{H}}(4),$$

and

$$\mu_{\mathcal{H}}(n) = \sum_{n_1=0}^{n} \sum_{n_2=0}^{n_1} \cdots \sum_{n_{N-1}=0}^{n_{N-2}} \binom{n}{n_1}\binom{n_1}{n_2} \cdots \binom{n_{N-2}}{n_{N-1}} \times M_{\delta_1}(n-n_1) M_{\delta_2}(n_1-n_2) \cdots \times M_{\delta_{N-1}}(n_{N-2}-n_{N-1}) M_{\delta_N}(n_{N-1})$$

where

$$M_{\delta_i}(n) = \frac{m_I^{-\frac{n}{2}}}{\Gamma(m_I)}\Gamma(1+n/2)\Gamma(m_I+n/2)$$

is the n-th moment of δ_i. For the case that $b^2-4ac \leq 0$, k_w and m_w are set to the estimated modulus values of the complex conjugate. Moreover, we assumed the channel gain $\mathcal{H}_d$ of direct link h_d as the K_G distribution, its PDF can be expressed by

$$f_{\mathcal{H}_d}(r|k_d, m_d, \Omega_d) \tag{18}$$

where k_d and m_d denote the shadowing parameter of direct path and Ω_d is the mean power of $\mathcal{H}_d$. Since the direct calculation of PDF of $\mathcal{H}$ is intractable, we follow the approximation approach of [24]. The sum of independent but not identically distributed (i.n.i.d.) K_G variables, in this case $\mathcal{H}_{RIS} + \mathcal{H}_d$, can be approximated by another K_G distribution with

$$m = k = \left[2\Omega^2 + \Omega(4\Omega^2 + 8\mathcal{S})^{-1/2}\right]/\mathcal{S}, \tag{19}$$

$\Omega = \sum_i \Omega_i$ where $\mathcal{S} = \sum_i AF_i\Omega_i$ calculated by using amount of fading $AF_i = \frac{1}{m_i} + \frac{1}{k_i} + \frac{1}{m_i k_i}$ for $i \in [w, d]$. Then, we finally obtain the approximated PDF of the received signal as

$$f_{\gamma_{\mathrm{RIS}}}(\gamma_{\mathrm{RIS}}) \approx \frac{2\Xi^{\zeta^+}\gamma_{\mathrm{RIS}}^{\frac{\zeta^+}{2}-1}K_{\zeta^-}(2\Xi\sqrt{\frac{\gamma_{\mathrm{RIS}}}{\bar{\gamma}_{\mathrm{RIS}}}})}{\Gamma(k)\Gamma(m)(\bar{\gamma}_{\mathrm{RIS}})^{\frac{\zeta^+}{2}}}, \tag{20}$$

where $\Xi = \sqrt{km/\Omega}$, $\zeta^- = k - m$ and $\zeta^+ = k + m$.

3. Performance Analysis

In this section, we provide a mathematical performance analysis of the RIS-assisted dual-hop mixed FSO-RF UAV communication system, focusing on outage probability, BER, and average capacity.

3.1. Outage probability

The outage probability of the considered system in this paper is expressed as

$$P_{\mathrm{out}} = \Pr(\min\{\gamma_{\mathrm{FSO}}, \gamma_{\mathrm{RIS}}\} \leq \gamma_{th}), \tag{21}$$

which can be rewritten as

$$P_{\mathrm{out}} = P_{\mathrm{out,FSO}} + P_{\mathrm{out,RIS}} - P_{\mathrm{out,FSO}}P_{\mathrm{out,RIS}}. \tag{22}$$

Using (7) and [25, Eq. (07.34.21.0084.01)] and letting $\tau = \gamma_{FSO}$, $\alpha = 1/2$, $\beta = 1$, $l = 1$, $k = 2$, $a = \gamma_{th}$ and algebraic manipulations, $P_{\mathrm{out,FSO}}$ is given by

$$P_{\mathrm{out,FSO}} = a_1 + \frac{C_1 2^{\alpha+\beta-3}\sqrt{\gamma_{th}}}{2\pi}G_{3,7}^{6,1}\left(\frac{C_2^2\gamma_{th}}{2^4}\middle|\begin{matrix}\kappa_1\\ \kappa_2\end{matrix}\right), \tag{23}$$

where $\kappa_1 = \frac{1}{2}, \frac{\tau}{2}, \frac{\tau+1}{2}$ and $\kappa_2 = \frac{\tau-1}{2}, \frac{\tau}{2}, \frac{\alpha-1}{2}, \frac{\alpha}{2}, \frac{\beta-1}{2}, \frac{\beta}{2}, -\frac{1}{2}$.

Moreover, using the Cumulative Distribution Function (CDF) approximation results of [23] and the fact that outage probability is equal to CDF, (20) can be approximated as

$$P_{\mathrm{out,RIS}} \simeq \frac{1}{\Gamma(k)\Gamma(m)}G_{1,3}^{2,1}\left[\frac{\Xi^2\gamma_{th}}{\bar{\gamma}_{\mathrm{RIS}}}\middle|\begin{matrix}1\\ k, m, 0\end{matrix}\right]. \tag{24}$$

In the high SNR regime, the end-to-end outage performance can be expressed by $P_{\mathrm{out}} \to P^A_{\mathrm{out,FSO}} + P^A_{\mathrm{out,RIS}}$. As SNR goes to infinity, the second term of (23) approaches zero. Therefore $P_{\mathrm{out,FSO}}$ can be approximated as

$$P^A_{\mathrm{out,FSO}} \approx a_1 = \exp\left(-\frac{\theta^2_{\mathrm{FOV}}}{2\left(\sigma^2_{to} + \sigma^2_{ro}\right)}\right). \tag{25}$$

Using [25, eq.(07.34.06.0006.01)] with letting $z = \frac{\Xi^2\gamma_{th}}{\bar{\gamma}_{\mathrm{RIS}}}$ and algebraic manipulation $P_{\mathrm{out,RIS}}$ can also be approximated as

$$P^A_{\mathrm{out,RIS}} \approx \frac{\Gamma(m-k)}{\Gamma(1+k)\Gamma(m)}\left(\frac{\Xi^2\gamma_{th}}{\bar{\gamma}_{\mathrm{RIS}}}\right)^k. \tag{26}$$

Since k is always larger than 1, the UAV-aided FSO link dominates the diversity gain. Finally, we obtain the asymptotic outage probability in the high SNR regime as

$$P_{\mathrm{out}} \to \exp\left(-\frac{\theta^2_{\mathrm{FOV}}}{2\left(\sigma^2_{to} + \sigma^2_{ro}\right)}\right). \tag{27}$$

Besides, the diversity gain of the proposed system can be analyzed by using (26) and (23) with [25, eq.(07.34.06.0006.01)] and algebraic manipulations. The diversity gain of the proposed system is as follows:

$$G_d = \min\left(0, \frac{\tau}{2}, \frac{\alpha}{2}, \frac{\beta}{2}, k\right).$$

Consequently, we can conclude that the overall diversity gain is 0. Moreover, focusing on more practical performance region where the most dominant contributor is not 0, the diversity gain can be drawn as follows by excluding 0:

$$G_{d,prac} = \min\left(\frac{\tau}{2}, \frac{\alpha}{2}, \frac{\beta}{2}, k\right).$$

3.2. BER

Using the relationship between the end-to-end BER of DF relaying protocol and BER of every single hop, the end-to-end BER of the considered system in this paper is given by [26]

$$P_{\mathrm{BER}} = P_{\mathrm{e,FSO}} + P_{\mathrm{e,RIS}} - 2P_{\mathrm{e,FSO}}P_{\mathrm{e,RIS}}, \tag{28}$$

where $P_{\mathrm{e,FSO}}$ and $P_{\mathrm{e,RIS}}$ denote BERs of the FSO link and the RIS-assisted RF link, respectively. Based on union bound, the BER of each link can be expressed as [27],

$$P_e = -\int_0^\infty F_\gamma(x)\, dP_b(x) \approx \frac{m_1 m_2}{2\sqrt{2\pi}} \int_0^\infty \frac{1}{\sqrt{x}} \exp\left(-\frac{m_2^2 x}{2}\right) F_\gamma(x)\, dx, \quad (29)$$

where $m_1 = 1$ and $m_2 = \sqrt{2}$ for binary phase shift Keying (BPSK) and $m_1 = \frac{4}{\log_2 M}$ and $m_2 = \sqrt{\frac{3}{M-1}}$ for M-ary quadrature amplitude modulation (M-QAM), respectively [28].

Using [29, eq.(7.813)], the BER of the FSO link is given by

$$P_{e,FSO} = \frac{a_1}{2} + \frac{C_1 2^{\alpha+\beta-2} m_1}{(2\pi)^{3/2} m_2} G_{4,7}^{6,2}\left(\frac{C_2^2}{2^3 m_2^2} \middle| \begin{matrix} \kappa_1' \\ \kappa_2 \end{matrix} \right), \quad (30)$$

where $\kappa_1' = (0, \kappa_1)$. Similarly, using [29, eq.(7.813)], the BER of the RIS-aided RF link is given by

$$P_{e,RIS} = \frac{1}{\Gamma(k)\Gamma(m)} \frac{m_1}{2\sqrt{\pi}} G_{2,3}^{2,2}\left[\frac{\Xi^2}{\bar{\gamma}_{RIS}} \frac{2}{m_2^2} \middle| \begin{matrix} 1/2, 1 \\ k, m, 0 \end{matrix} \right]. \quad (31)$$

The asymptotic BER performance in a high SNR regime can be expressed by $P_{BER} \to P_{e,FSO}^A + P_{e,RIS}^A$. Using a similar approach of the asymptotic analysis for outage probability with [25, eq.(07.34.06.0006.01)], we have

$$P_{e,FSO}^A \approx \frac{a_1}{2} = \frac{1}{2} \exp\left(-\frac{\theta_{FOV}^2}{2\left(\sigma_{to}^2 + \sigma_{ro}^2\right)} \right). \quad (32)$$

Using [25, eq.(07.34.06.0006.01)], $P_{e,RIS}$ can be approximated as

$$P_{e,RIS} \approx \frac{\Gamma(m-k)}{2\Gamma(k)} \left(\frac{\Xi^2 \gamma_{th}}{\bar{\gamma}_{RIS}} \right)^k. \quad (33)$$

Since k is always larger than 1, the first hop FSO link dominates the diversity gain. Finally, we obtain the asymptotic BER in high SNR regime as

$$P_{BER} \to \frac{1}{2} \exp\left(-\frac{\theta_{FOV}^2}{2\left(\sigma_{to}^2 + \sigma_{ro}^2\right)} \right). \quad (34)$$

3.3. Average Capacity

To provide analytic insight into the considered system, we investigate its average (ergodic) capacity. The average capacity of the mixed dual-hop FSO-RF UAV communication system is given by

$$C_{avg} = \frac{1}{2} \mathbb{E}\{\log_2(1 + \min(\gamma_{FSO}, \gamma_{RIS}))\}. \quad (35)$$

Let $C_{FSO} = \log_2(1 + \gamma_{FSO})$ and $C_{RIS} = \log_2(1 + \gamma_{RIS})$. Then, using following relationship $\mathbb{E}\{\log_2(1 + \min(\gamma_{FSO}, \gamma_{RIS}))\} = \mathbb{E}\{\min(C_{FSO}, C_{RIS})\} = \min(\mathbb{E}\{\min(C_{FSO}, C_{RIS})\}) \le \min(\mathbb{E}\{C_{FSO}\}, \mathbb{E}\{C_{RIS}\})$, the C_{avg} can be upper bounded by

$$C_{avg} \le \frac{1}{2} \min(\mathbb{E}\{C_{FSO}\}, \mathbb{E}\{C_{RIS}\}), \quad (36)$$

where

$$\mathbb{E}\{C_{FSO}\} = \frac{1}{\ln(2)} \int_0^\infty \ln(1 + \gamma_{FSO}) f_{\gamma_{FSO}}(\gamma_{FSO}) \quad (37)$$

and

$$\mathbb{E}\{C_{RIS}\} = \frac{1}{\ln(2)} \int_0^\infty \ln(1 + \gamma_{RIS}) f_{\gamma_{RIS}}(\gamma_{RIS}), \quad (38)$$

which denote the average capacity of the FSO and the RIS-aided RF links, respectively. From [25, eq. (07.34.03.0456.01)] we have $\ln(1+\gamma) = G_{2,2}^{1,2}\left[\gamma\middle|_{1,0}^{1,1}\right]$, letting $\alpha = 1/2$, $\sigma = 1$, $\omega = C_2$, $l = 1$, $k = 2$ and algebraic manipulations with using [25, eq. (07.34.21.0013.01)] we have

$$\mathbb{E}\{C_{FSO}\} = \frac{2^{\alpha+\beta-3}}{2\pi} \frac{C_1}{\ln(2)} G_{4,8}^{8,1}\left(\frac{C_2^2}{2^4} \middle| \begin{matrix} \kappa_1'' \\ \kappa_2' \end{matrix} \right), \quad (39)$$

where $\kappa_1'' = (-\frac{1}{2}, \kappa_1)$ and $\kappa_2' = (\kappa_2, -\frac{1}{2})$.

Moreover, from [25, eq. (03.04.26.0009.01)] we have $K_\nu(\sqrt{z}) = \frac{1}{2} G_{0,2}^{2,0}\left[\frac{z}{4}\middle| \frac{\nu}{2}, -\frac{\nu}{2}\right]$, and using [25, eq. (07.34.21.0011.01)], the average capacity of RIS-aided RF link can be written as

$$\mathbb{E}\{C_{RIS}\} = \frac{\Xi^{\zeta^+}}{\ln(2)\Gamma(k)\Gamma(m)(\bar{\gamma}_{RIS})^{\frac{\zeta^+}{2}}} G_{2,4}^{4,1}\left[\frac{\Xi^2}{\bar{\gamma}_{RIS}} \middle| \begin{matrix} \mu_1 \\ \mu_2 \end{matrix} \right] \quad (40)$$

where $\mu_1 = -\frac{\zeta^+}{2}, 1 - \frac{\zeta^+}{2}$ and $\mu_2 = \frac{\zeta^-}{2}, -\frac{\zeta^-}{2}, -\frac{\zeta^+}{2}, \frac{\zeta^+}{2}$.

4. Simulation Results

In this section, we validate our mathematical analysis through extensive computer simulations. The simulation parameters are summarized as follows: $D_{FSO} = 250$m, $\zeta = 0.01$, $r_a = 5$cm, $\sigma_{tp} = \sigma_{rp} = 0.3$m, $\sigma_{to} = \sigma_{ro} = 3$mrad, $\theta_{FOV} = 15$mrad, $\sigma_R^2 = 0.1$, $\gamma_{th} = 6.8$dB. We presented simulation results for large transmit SNR difference assumption between RIS and FSO link of $\bar{\gamma}_{RIS} = \bar{\gamma}_{FSO} - 30$dB to show more dynamic region of performance. Typically, FSO links require higher SNRs compared to RF links, while RIS-assisted RF links are more efficient in terms of SNR. Therefore, our assumption is reasonable for mixed FSO and RIS-assisted RF scenarios. The simulation parameters for the UAV FSO link are adopted from [10], while those for the RF link are configured to reflect practical mixed LoS and non-LoS channel conditions. Extensive simulation results are presented in the following two subsections. In the first subsection, we present the simulation results for the proposed system *without* a direct path, i.e., by setting $h_d = 0$ in (12). Subsequently, we present the simulation results for the proposed system *with* a direct path.

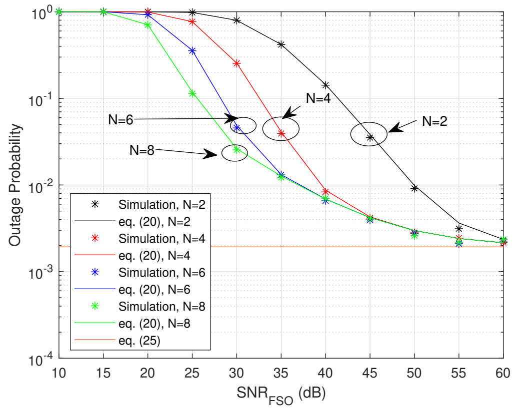

Fig. 2. Outage probability for varying SNR of the FSO link when $N = 2, 4, 6, 8$ and without direct path.

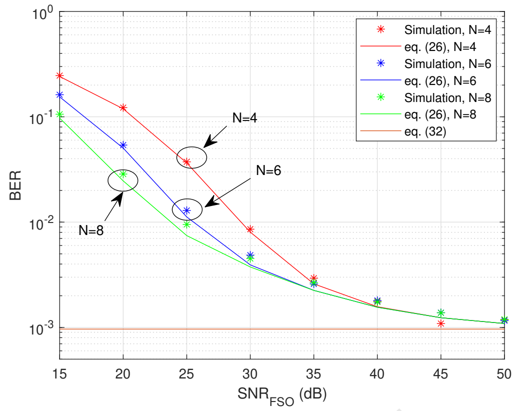

Fig. 4. BER of the FSO link with BPSK for varying SNR (without direct path).

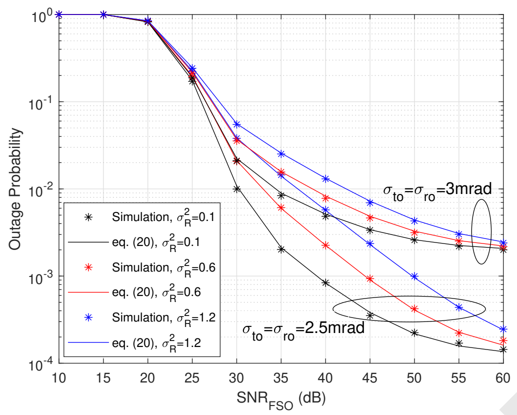

Fig. 3. Outage probability for varying SNR of the FSO link with various Rytov and orientation variances when $N = 7$ and without direct path.

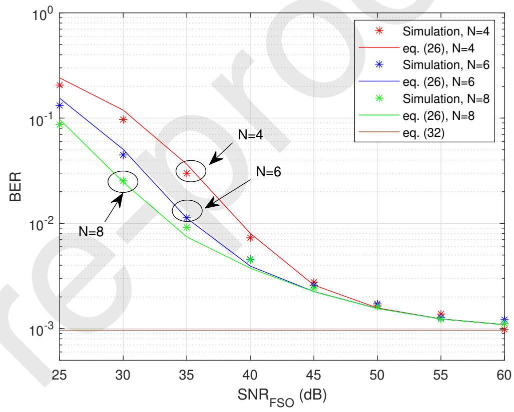

Fig. 5. BER of the FSO link with BPSK for varying SNR (without direct path).

4.1. Without Direct Path

Figure 2 shows the outage probability of the proposed system for varying SNRs of the FSO link, considering cases with 2, 4, 6, and 8 RIS elements and without a direct path. The results demonstrate that the analytical findings closely match the simulation results. As expected, increasing the number of RIS elements (N) improves outage performance. However, the outage probability eventually saturates at a certain value as N and SNR increase, because the overall performance becomes dominated by the FSO link. Figure 3 presents the outage probability of the proposed system for various Rytov and orientation variation values with $N = 7$. The results indicate that the analytical findings closely align with the simulation results. As shown in (27), the saturated outage probability is influenced by σ_{to} and σ_{ro}.

Figures 4 and 5 show the BER of the proposed system without a direct path for BPSK and 16QAM modulations, with $N = 2, 4, 6, 8$, $m_I = 1$, and $\sigma_R = 1$. The results demonstrate that the mathematical analysis of the BER closely matches the simulation results, regardless of the number of RIS elements. Similar to the outage probability, the BER saturates at a specific value as N and SNR increase, which is influenced by σ_{to} and σ_{ro}. The physical intuition behind the saturation of outage and BER performance lies in the characteristics of FSO links. The Field of View (FOV) of the FSO lens is significantly narrower than the beamwidth of an RF antenna. Furthermore, if the signal falls outside the FOV, it can no longer be recovered. As a result, position and orientation error variances become critical factors affecting performance, leading to tracking errors on the receiver side. This limitation causes the performance to saturate at a certain level in the high SNR regime.

Figure 6 illustrates the average capacity of the proposed system for varying SNRs of the FSO link with $N = 2, 4, 6, 8$, $m_I = 1$, and $\sigma_R = 0.1$. The analyzed upper bound of the average capacity shows excellent agreement with the simulation results across all SNR values, including scenarios with a small number of RIS elements, where Gaussian approximation-based performance analysis typically exhibits a significant gap compared to simulation results [12].

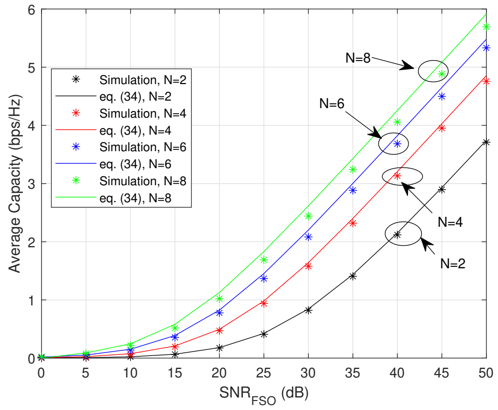

Fig. 6. Average capacity of the FSO link for varying SNR (without direct path).

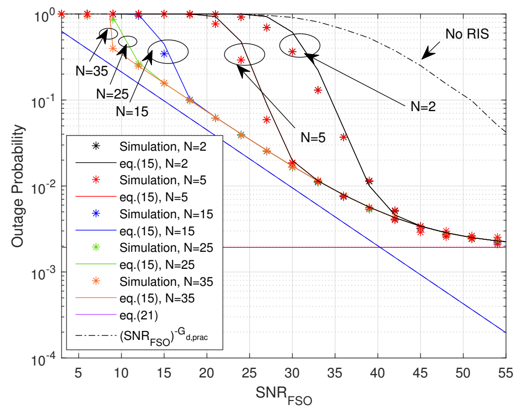

Fig. 7. Outage probability of the FSO link with a direct path for varying SNR when $N = 2, 5, 15, 25, 35$.

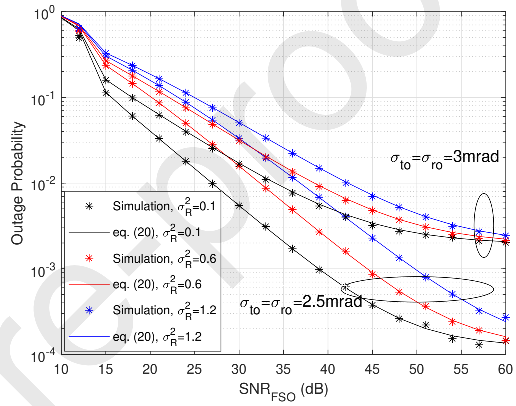

Fig. 8. Outage probability of the FSO link with a direct path for varying SNR for various Rytov and orientation variances when $N = 20$.

4.2. With Direct Path

Figure 7 depicts the outage probability of the proposed system for varying SNRs of the FSO link with a direct RF path, considering 2, 5, 15, and 25 RIS elements and parameters $m_I = 5$, $m_d = 2$, and $k_d = 5$. The results indicate that the analytical predictions closely align with the simulation outcomes. As expected, increasing the number of RIS elements (N) improves the outage performance. However, the outage probability eventually saturates at a specific value as N and SNR increase, as the overall performance becomes dominated by the FSO link. Figure 8, illustrates the outage probability for varying SNRs of the FSO link with different Rytov and orientation variances when $N = 20$, $m_I = 5$, $m_d = 2$, and $k_d = 5$. The results demonstrate that the outage analysis remains consistent with the simulation results across various values of σ_R^2, σ_{to}, and σ_{ro}. Notably, the saturated outage probability is influenced by σ_{to} and σ_{ro}.

Figure 9 shows the outage probability for varying SNRs of the FSO link with different scattering factors (ζ) and FSO link distances (D_{FSO}) when $N = 4$ with a direct link. The results indicate that the simulation and analytical predictions align well, even when the distance between UAVs changes. However, a noticeable discrepancy arises when the scattering factor is set to an unrealistically large value. Since such extreme scattering values are not practical [30], the presented analysis can be considered a good match for realistic scenarios. Figure 10 presents the outage probability for varying SNRs of the FSO link under different schemes. First, the case of DF relaying without RIS shows very poor outage performance due to the lack of performance enhancement from the RIS. Next, the results for RIS-assisted DF relaying systems are shown for scenarios with and without direct paths in each RF link. For comparison, we also include a single-hop UAV-to-UAV FSO communication scenario. When the RF link performs well, the FSO link becomes the performance bottleneck. Additionally, we examine a single-hop fixed FSO communication scenario, where no performance saturation occurs, unlike UAV-based FSO links. In this case, the outage performance improves significantly as the SNR increases.

Figure 11 presents simulation results based on a practical distance-dependent path-loss model for the RIS/RF link, providing deeper insight into the proposed system model. The path-loss model adopted is described in [31, 32]. According to this model, the noise power is calculated as: $\sigma_{\mathrm{D}}^2 = N_0 + 10\log(\mathrm{BW}) + \mathrm{NF}$, where the noise power density is set to $N_0 = -147dBm/Hz$, the signal bandwidth is $BW = 10MHz$, and the noise figure is $\mathrm{NF} = 7dB$. The path-loss model used is as follows:

$$\beta(d)[\mathrm{dB}] = G_{\mathrm{t}}+G_{\mathrm{r}}+\begin{cases} -37.5 - 22\log_{10}(d) & \text{if LOS,} \\ -35.1 - 36.7\log_{10}(d) & \text{if NLOS,} \end{cases}$$

where d is the distance in meters, and the antenna gains are $G_{\mathrm{R}} = 8$, $G_{\mathrm{RIS_n}} = 8$, and $G_{\mathrm{D}} = 0$ in dB scale for the relay (R), n-th RIS element, and destination (D), respectively. Additionally, d_{RN}, d_{ND}, and d_{RD} represent the distances between the relay and RIS, RIS and destination, and relay and destination, respectively, all in meters. The value of d_{RD} can be calculated

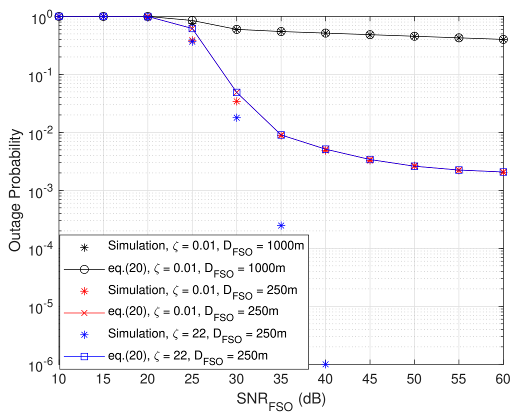

Fig. 9. Outage probability of the FSO link with direct link for varying SNR in various scattering factor ζ and FSO link distance D_{FSO} when N=4.

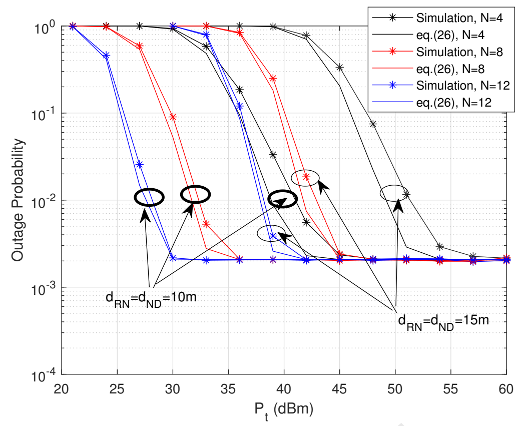

Fig. 11. Outage Probability of the FSO link with direct path for varying transmission power.

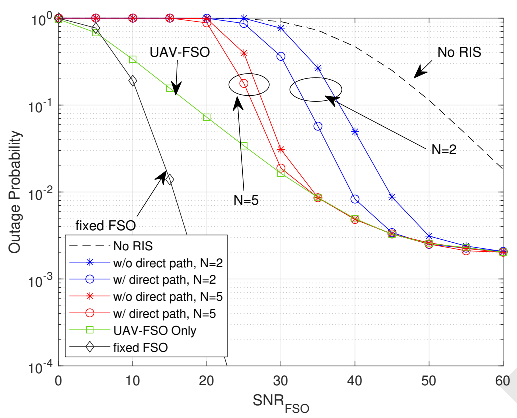

Fig. 10. Outage probability of the FSO link for varying SNR.

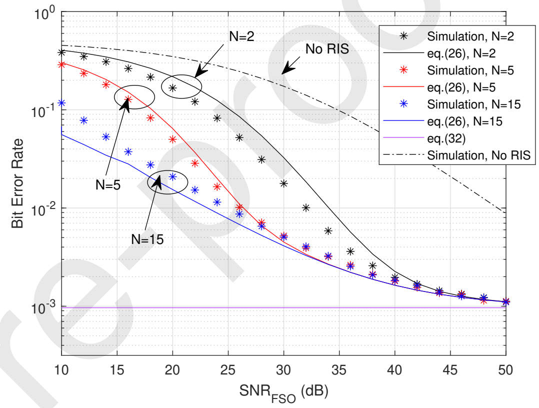

Fig. 12. BER of the FSO link with BPSK for varying SNR (with direct path).

using d_{RN}, d_{ND}, and the angle θ_{R_D} between the relay-RIS and RIS-destination, which is set to 80 degrees in this paper. Based on these assumptions, the outage performance of the proposed system is evaluated. The results reveal that the outage performance is strongly influenced by the distances between the nodes.

Figures 12 and 13 depict the BER of the proposed system for BPSK and 16QAM modulations, with $N = 2, 5, 15$, $m_I = 1.2$, $m_d = 2$, $k_d = 5$, and $\sigma_R = 1$. The mathematical analysis of the BER closely aligns with the simulation results, with variations depending on the number of RIS elements. Specifically, the performance gap between the analysis and simulation results is less than 2dB for $N = 2$ and less than 1dB for $N = 15$. For $N = 5$, the gap is minimal. These results demonstrate that increasing the number of RIS elements significantly enhances BER performance. Similar to the outage probability, the BER saturates at a specific value as N and SNR increase, influenced by σ_{to} and σ_{ro}.

Figure 14 illustrates the average capacity of the proposed system for varying SNRs of the FSO link with $N = 2, 5, 15, 25$, $m_I = 3$, $m_d = 2$, $k_d = 5$, and $\sigma_R = 0.1$. The results show that the derived upper bound for the average capacity is highly accurate across all SNR values, particularly when the number of RIS elements is small. Notably, the average capacity improves significantly as the number of RIS elements increases.

5. Conclusion

In this paper, we presented a mathematical performance analysis of a RIS-assisted mixed dual-hop FSO-RF UAV-aided communication system, focusing on outage probability, BER, and average capacity. The analytical results were validated against computer simulations, demonstrating a strong agreement. Our findings indicate that RIS can significantly enhance the end-to-end performance of the system, as evidenced by both mathematical analysis and simulation results. However, the impact of UAV hovering on system performance becomes dominant when the RIS-assisted RF link performs exceptionally well. Notably, the derived mathematical expressions for outage probability, BER, and average capacity represent the first analytical results reported in the literature for this type of system, to the best of our knowledge.

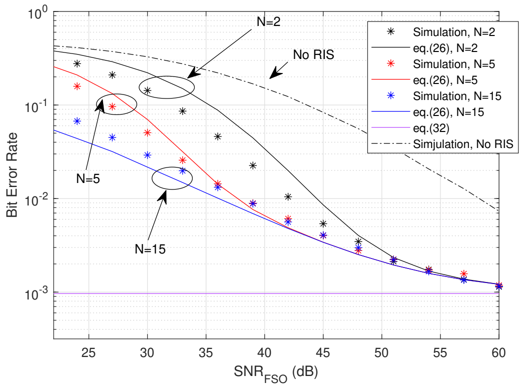

Fig. 13. BER of the FSO link with 16QAM for varying SNR (with direct path).

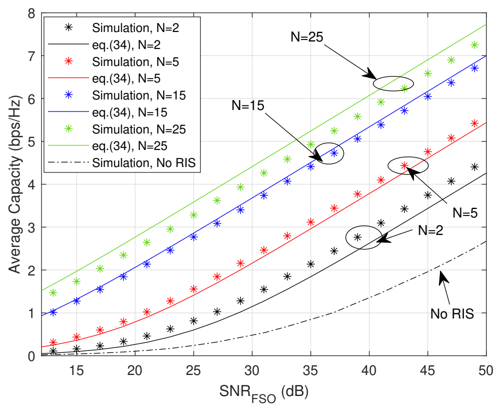

Fig. 14. Average capacity of the FSO link with direct path for varying SNR.

Acknowledgements

This research was supported in part by the MSIT (Ministry of Science and ICT), Korea, under the ITRC (Information Technology Research Center) support program (IITP-2024-RS-2024-00436406) supervised by the IITP (Institute for Information & Communications Technology Planning & Evaluation), in part by the Institute for Information and Communications Technology Promotion (IITP) Grant funded by the Korea Government (MSIP, Development of Cube Satellites Based on Core Technologies in Low Earth Orbit Satellite Communications) under Grant RS-2024-00396992, and in part by the Korea Research Institute for Defense Technology planning and advancement (KRIT) grant, funded by the Korea government (DAPA (Defense Acquisition Program Administration)) (21-106-A00-007, Space-Layer Intelligent Communication Network Laboratory, 2022).

References

[1] E. Basar, M. Di Renzo, J. De Rosny, M. Debbah, M.-S. Alouini, R. Zhang, Wireless communications through reconfigurable intelligent surfaces, IEEE Access 7 (2019) 116753–116773.

[2] Q. Wu, R. Zhang, Towards smart and reconfigurable environment: Intelligent reflecting surface aided wireless network, IEEE Communications Magazine 58 (1) (2020) 106–112.

[3] L. Yang, W. Guo, I. S. Ansari, Mixed dual-hop FSO-RF communication systems through reconfigurable intelligent surface, IEEE Communications Letters 24 (7) (2020) 1558–1562.

[4] L. Yang, F. Meng, J. Zhang, M. O. Hasna, M. D. Renzo, On the performance of RIS-assisted dual-hop UAV communication systems, IEEE Transactions on Vehicular Technology 69 (9) (2020) 10385–10390.

[5] X. Liu, J. Zou, W. Xie, X. Peng, C. Li, Performance analysis of RIS-assisted mixed dual-hop FSO-RF communication systems over exponentiated Weibull channels, Security and Communication Networks (2021) (2021) 1–7.

[6] Z. Zhu, Z. Li, Z. Chu, Y. Guan, Q. Wu, P. Xiao, M. D. Renzo, I. Lee, Intelligent reflecting surface assisted mmwave integrated sensing and communication systems, IEEE Internet of Things Journal 11 (18) (2024) 29427–29437.

[7] R. Liu, K. Guo, X. Li, K. Dev, S. A. Khowaja, T. A. Tsiftsis, H. Song, RIS-empowered satellite-aerial-terrestrial networks with PD-NOMA, IEEE Communications Surveys & Tutorials 26 (4) (2024) 2258 – 2289.

[8] M. Alzenad, M. Z. Shakir, H. Yanikomeroglu, M.-S. Alouini, FSO-based vertical backhaul/fronthaul framework for 5G+ wireless networks, IEEE Communications Magazine 56 (1) (2018) 218–224.

[9] E. Lee, J. Park, D. Han, G. Yoon, Performance analysis of the asymmetric dual-hop relay transmission with mixed RF/FSO links, IEEE Photonics Technology Letters 23 (21) (2011) 1642–1644.

[10] G. Xu, S. Lu, L. Qu, Q. Zhang, Z. Song, B. Ai, Outage probability and average BER of UAV-Assisted RF/FSO system for space-air-ground integrated networks under angle-of-arrival fluctuations, IEEE Internet of Things Journal 11 (20) (2024) 34009 – 34023.

[11] M. T. Dabiri, S. M. S. Sadough, I. S. Ansari, Tractable optical channel modeling between UAVs, IEEE Transactions on Vehicular Technology 68 (12) (2019) 11543–11550.

[12] L. Yang, F. Meng, Q. Wu, D. B. da Costa, M.-S. Alouini, Accurate closed-form approximations to channel distributions of RIS-aided wireless systems, IEEE Wireless Communications Letters 9 (11) (2020) 1985–1989.

[13] X. Huang, J. A. Zhang, R. P. Liu, Y. J. Guo, L. Hanzo, Airplane-aided integrated networking for 6G wireless: Will it work?, IEEE Vehicular Technology Magazine 14 (3) (2019) 84–91.

[14] M. T. Dabiri, S. M. S. Sadough, M. A. Khalighi, Channel modeling and parameter optimization for hovering UAV-based free-space optical links, IEEE Journal on Selected Areas in Communications 36 (9) (2018) 2104–2113.

[15] V. R. Nallagonda, P. Krishnan, Performance analysis of FSO based inter-UAV communication systems, Optical and Quantum Electronics 53 (4).

[16] M. Di Renzo, K. Ntontin, J. Song, F. H. Danufane, X. Qian, F. Lazarakis, J. De Rosny, D.-T. Phan-Huy, O. Simeone, R. Zhang, M. Debbah, G. Lerosey, M. Fink, S. Tretyakov, S. Shamai, Reconfigurable intelligent surfaces vs. relaying: Differences, similarities, and performance comparison, IEEE Open Journal of the Communication Society 1 (2020) 798–807.

[17] X. Pang, M. Sheng, N. Zhao, J. Tang, D. Niyato, K.-K. Wong, When UAV meets IRS: Expanding air-ground networks via passive reflection, IEEE Wireless Communications 28 (5) (2021) 164–170.

[18] M. Hua, L. Yang, Q. Wu, C. Pan, C. Li, A. L. Swindlehurst, UAV-assisted intelligent reflecting surface symbiotic radio system, IEEE Transactions on Wireless Communications 20 (9) (2021) 5769–5785.

[19] D. Singh, S. R, Comprehensive performance analysis of hovering UAV-based FSO communication system, IEEE Photonics Journal 14 (5) (2022) 1–13.

[20] O. S. Badarneh, M. K. Awad, S. Muhaidat, F. S. Almehmadi, Performance analysis of intelligent reflecting surface-aided

decode-and-forward UAV communication systems, IEEE Systems Journal 17 (1) (2023) 246–257.

[21] G. Xu, Z. Song, Performance analysis of a UAV-assisted RF/FSO relaying systems for internet of vehicles, IEEE Internet of Things Journal 9 (8) (2022) 5730–5741.

[22] A. M. Hunter, J. G. Andrews, S. Weber, Transmission capacity of ad hoc networks with spatial diversity, IEEE Transactions on Wireless Communications 7 (12) (2008) 5058–5071.

[23] K. P. Peppas, Accurate closed-form approximations to generalised-K sum distributions and applications in the performance analysis of equal-gain combining receivers, IET Communications 5 (7) (2011) 982–989.

[24] G. N. Kamga, M. Xia, S. Aïssa, A unified performance evaluation of integrated mobile satellite systems with ancillary terrestrial component, in: Proceedings of the 2015 IEEE International Conference on Communications, IEEE, 2015, pp. 934–938.

[25] Wolfram, The wolfram functions site. [online].
URL `http://functions.wolfram.com`

[26] O. M. S. Al-Ebraheemy, A. M. Salhab, A. Chaaban, S. A. Zummo, M.-S. Alouini, Precise performance analysis of dual-hop mixed RF/Unified-FSO DF relaying with heterodyne detection and two IM-DD channel models, IEEE Photonics Journal 11 (1) (2019) 1–22.

[27] S. Anees, M. R. Bhatnagar, Performance of an amplify-and-forward dual-hop asymmetric RF–FSO communication system, Journal of Optical Communications and Networking 7 (2) (2015) 124–135.

[28] J. G. Proakis, Digital communications, New York: McGraw Hill, 2007.

[29] I. S. Gradshteyn and I. M. Ryzhik, Table of integrals, series, and products, 7th, Academic, 2007.

[30] P. Demir, G. Yılmaz, Investigation of the atmospheric attenuation factors in FSO communication systems using the taguchi method, International Journal of Optics 2020.

[31] E. Bjornson, O. Ozdogan, E. G. Larsson, Intelligent reflecting surface versus decode-and-forward: How large surfaces are needed to beat relaying?, IEEE Wireless Communications Letters 9 (2) (2020) 244–248.

[32] V.-D. Phan, B. C. Nguyen, T. M. Hoang, T. N. Nguyen, P. T. Tran, B. V. Minh, M. Voznak, Performance of cooperative communication system with multiple reconfigurable intelligent surfaces over Nakagami-*m* fading channels, IEEE Access 10 (2022) 9806–9816.

Declaration of interests

☒ The authors declare that they have no known competing financial interests or personal relationships that could have appeared to influence the work reported in this paper.

☒The authors declare the following financial interests/personal relationships which may be considered as potential competing interests: